$KCa_4(BO_3)_3:Ln^{3+}$ (Ln = Dy, Eu, Tb) phosphors for near UV excited white–light–emitting diodes

Allu Amarnath Reddy, Subrata Das, Ashutosh Goel, Rupam Sen, Renée Siegel, Luís Mafra, G. Vijaya Prakash, and José M. F. Ferreira'

Citation: AIP Advances **3**, 022126 (2013); doi: 10.1063/1.4794189
View online: http://dx.doi.org/10.1063/1.4794189
View Table of Contents: http://aip.scitation.org/toc/adv/3/2
Published by the American Institute of Physics

AIP ADVANCES **3**, 022126 (2013)

$KCa_4(BO_3)_3$:Ln^{3+} (Ln = Dy, Eu, Tb) phosphors for near UV excited white–light–emitting diodes

Allu Amarnath Reddy,[1,2] Subrata Das,[2,3] Ashutosh Goel,[1,4] Rupam Sen,[5] Renée Siegel,[5] Luís Mafra,[5] G. Vijaya Prakash,[2] and José M. F. Ferreira[1,a]
[1]*Department of Materials and Ceramics Engineering, University of Aveiro, CICECO, 3810–193 Aveiro, Portugal*
[2]*Nanophotonics Laboratory, Department of Physics, Indian Institute of Technology Delhi, New Delhi, 110016, India*
[3]*Department of Chemical Engineering, National Taiwan University, Taipei, Taiwan, R.O.C*
[4]*Sterlite Technologies Ltd., E–1, E–2, E–3, MIDC, Waluj, Aurangabad 431136, Maharashtra, India*
[5]*Department of Chemistry, University of Aveiro, CICECO, 3810–193 Aveiro, Portugal*

(Received 21 September 2012; accepted 14 February 2013; published online 28 February 2013)

A series of doped $KCa_4(BO_3)_3$:Ln^{3+} (Ln: Dy, Eu and Tb) compositions were synthesized by solid–state reaction method and their photoluminescent properties were systematically investigated to ascertain their suitability for application in white light emitting diodes. The X–ray diffraction (XRD) and nuclear magnetic resonance (MAS–NMR) data indicates that Ln^{3+}–ions are successfully occupied the non–centrosymmetric Ca^{2+} sites, in the orthorhombic crystalline phase of $KCa_4(BO_3)_3$ having space group *Ama2*, without affecting the boron chemical environment. The present phosphor systems could be efficiently excitable at the broad UV wavelength region, from 250 to 350 nm, compatible to the most commonly available UV light–emitting diode (LED) chips. Photoluminescence studies revealed optimal near white–light emission for $KCa_4(BO_3)_3$ with 5 wt.% Dy^{3+} doping, while warm white–light (CIE; X = 0.353, Y = 0.369) is obtained at 1wt.% Dy^{3+} ion concentration. The principle of energy transfer between Eu^{3+} and Tb^{3+} also demonstrates the potential white–light from $KCa_4(BO_3)_3$:Eu^{3+},Tb^{3+} phosphor. Whereas, single Tb^{3+} and Eu^{3+}–doped systems showed bright green (Tb^{3+}) and red (Eu^{3+}) emissions, respectively. Having structural flexibility along with remarkable chemical/thermal stability and suitable quantum efficiency these phosphors can be promising candidates as white–light–emitter for near UV LEDs. *Copyright 2013 Author(s). This article is distributed under a Creative Commons Attribution 3.0 Unported License.* [http://dx.doi.org/10.1063/1.4794189]

I. INTRODUCTION

Recent years have witnessed an upsurge in the research and development of white–light emitting diodes (W–LEDs) being known for general illumination sources due to their unmatchable benefits, for example: high brightness, longer lifetime, small volume, and low power consumption. Being mercury–free, they are expected to be a viable replacement for conventional luminescent and fluorescent lamps in the near future.[1–6]

One of the most fashionable approaches to produce white light is uniting a blue InGaN based LED with a broadband yellow–emitting $Y_3Al_5O_{12}$:Ce^{3+} (YAG) phosphor. However, this system lacks thermal stability at higher temperatures above 150 °C. Also, the resultant white light exhibits low color rendering index (R_a) due to lack of individual blue, red and green region colors.[7–9] Uniform white–light with high R_a can be alternatively achieved by mixing several single color

[a]Corresponding author Tel.: +351–234–370242; Fax: +351–234–370204. E–mail address: jmf@ua.pt (J.M.F. Ferreira)

emitting phosphors with UV–LEDs.[10,11] $BaMgAl_{10}O_{17}:Eu^{2+}$ ($BAM:Eu^{2+}$) and $BaMgAl_{10}O_{17}:Mn^{2+}$ ($BAM:Mn^{2+}$) are some of the well-known blue and green phosphors broadly used for the generation of white–light because of their high emission efficiency at vacuum UV excitation (VUV) and prominent R_a.[12,13] However, despite many advantages, the final phosphor product suffers from complexities associated with the combination of several phosphors used in the fabrication and its significant degradation during heating, which reduce the lifetime and efficiency of WLEDs.[10,11,14]

The pursuit in this direction has led to identify new class of phosphors having broadband near white emitting properties based on oxides,[15–18] oxyfluorides,[19,20] nitrides,[21,22] oxynitrides,[23–25] sulfides[26,27] and halides.[28,29] Among all, the oxyfluoride (for example: $Sr_{2.975-x}–Ba_xCe_{0.025}AlO_4F$) phosphors have been seen with alacrity as the most efficient matrix for photoluminescence due to their low phonon energy.[19,20] Such low phonon energies are expected to decrease the contribution of non–radiative multi–phonon relaxations during the emission process of dopant rare–earth ions, resulting into enhancement of net emission quantum efficiency.[19,20] However, despite of the high quantum efficiency, fluoride based phosphor systems are very moisture sensitive in nature, thus raising concerns regarding their practical applications.[20] Therefore single–host broad band emitting phosphors need to be developed for low–cost W–LEDs with improved chemical and thermal stability better reproducibility and a simpler fabrication process.[10,11]

With the above mentioned perspectives, the present article focuses on studying the influence of rare–earth doping/co–doping on the luminescence properties of borate based phosphors. Owing to their simple and low–cost fabrication along with high thermal and chemical stability as well as transparency over a wide spectral range (beginning from UV and extending into visible)[5,11] borate hosts are considered as potential candidates for many potential optoelectronic applications, particularly in the field of laser science and technology.[11] The most known borate phosphors include $M_3Al_6B_8O_{24}:Ce^{3+}$(M = Ca,Sr,Ba),[30] $YCa_3(AlO)_3(BO_3)_4:Eu^{3+}$,[31] $Na_2Y_2B_2O_7:Eu^{3+}$,[31] $Sr_3Y_2(BO_3)_4:Eu^{3+}$,[32] $Sr_2Mg(BO_3)_2:Ce^{3+}$,[33] $NaSr_4(BO_3)_3:Ce^{3+},Mn^{2+}$,[34] $Na_2Gd_2B_2O_7:Ce^{3+}$, Tb^{3+},[35] and $NaSrBO_3:Ce^{3+}$.[5] The aim of the present research is to develop borate (containing planar $[BO_3]^{3-}$ groups) based phosphors having the quality of near white light emission, since borate hosts exhibited excellent thermal stability over the commercial YAG host,[5] and they are less moisture sensitive in nature than the usual oxyfluoride hosts.[5,20] Very recently, we have successfully demonstrated promising near white–light emission from $KCaBO_3:Dy^{3+},Eu^{3+}$ phosphor upon blue excitation.[11] The $KCaBO_3$ systems are found to be attractive since the enhanced luminescence properties are observed due to the occupation of large concentrations of DY^{3+}/Eu^{3+} ions into the Ca^{2+} ions by the preferential charge-compensation mechanism of $2Ca^{2+} = Dy^{3+}/Eu^{3+} + K^+$.

The present structurally attractive $KCa_4(BO_3)_3$ host having strong absorption in the UV/near–UV (NUV) regions is expected to enhance the energy transfer process efficiency from host lattice to the activator upon NUV excitations. It is worth mentioning that the crystal structure of $KCa_4(BO_3)_3$ has been firstly reported by Wu *et al.*[36] But, to the best of our knowledge, luminescence properties of rare–earth ion doped $KCa_4(BO_3)_3$ phosphors and corresponding applications for W–LEDs are not been reported in the literature. For white–light generation, Dy^{3+} ion doping is a popular choice, due to the combined emission from strong blue (B, $^4F_{9/2} \rightarrow {}^6H_{15/2}$) and yellow (Y, $^4F_{9/2} \rightarrow {}^6H_{13/2}$) emission bands. Particularly, the Dy^{3+} ion emission show strong crystal field effects, therefore intensity of hypersensitive yellow color emission from the transition $^4F_{9/2} \rightarrow {}^6H_{13/2}$ is strongly influenced by the host environment, compared to the other non-hypersensitive emission band $^4F_{9/2} \rightarrow {}^6H_{15/2}$.[11,37,38] Hence, it is interesting to observe such host matrix influence on the near-white light generation from Dy^{3+}–doped phosphors directly by fine tuning the ratio of these yellow and blue prominent emission intensities.[37,38] We have also developed Eu^{3+} and Tb^{3+} singly and co–doped systems for red and green emission components for the generation of white–light. Nevertheless, these combinations can be interesting candidates to combine with UV/NUV light for realizing white–light with suitable color rendering index.

Eventually, Dy^{3+}–singly doped and Eu^{3+}/Tb^{3+}–codoped $KCa_4(BO_3)_3$ phosphors were synthesized by a solid–state reaction method and their emission spectra were obtained under NUV excitations in order to search for new compositions for white light phosphors. Intense white light was obtained in $KCa_4(BO_3)_3:Dy^{3+}$, while Eu^{3+}/Tb^{3+}–codoped $KCa_4(BO_3)_3$ phosphor showed near

white light emission under the excitation of 350 nm. Based on the above referred findings, the focus has now been extended to the energy transfer mechanism, emission quenching and color rendering properties of the synthesized $KCa_4(BO_3)_3$ phosphors.

II. EXPERIMENTAL DETAILS

The synthesis of various concentrations of Ln^{3+} (Ln: Dy, Eu & Tb)–doped $KCa_4(BO_3)_3$ phosphors is accomplished from solid state reaction. Stoichiometric amounts of analytical grade K_2CO_3, $CaCO_3$, H_3BO_3, Dy_2O_3, Tb_2O_3 and Eu_2O_3 were mixed and ground well in an agate mortar to obtain a fine and homogeneous powder. The mixture was then annealed in a furnace in air atmosphere at 800 ^oC for 7 h in alumina boats and cooled to room temperatures.

X–ray diffraction (XRD) patterns for these powders were collected by Rigaku Geigerflex D/Max, C Series, Tokyo, Japan; with Cu K_α radiation ($\lambda = 1.54$ Å) in the 2θ angle range 10^o–80^o with step size 0.02^o/s.

Scanning electron microscopy (SEM; SU–70, Hitachi) attached with energy dispersive spectroscopic detection system (EDS; Bruker Quantax, Germany) was used to study the morphology and the distribution of individual atomic constituents.

^{11}B NMR experiments were carried out on a Bruker Avance–III operating at a Larmor frequency of 128.38 MHz ($B_0 = 9.4$ T) and using a 4 mm double resonance probe. A solution of boric acid was used for the chemical shift reference and to set–up the radio–frequency (RF) field strength. ^{11}B MAS NMR spectra were acquired using a pulse length of 1.0 μs and a RF field strength of 45 kHz at a spinning rate (ν_R) of 10.0 kHz with a recycling delay of 120 s. Two–dimensional (2D) t1–split Satellite Transition Magic Angle Spinning (STMAS)[39] spectrum was recorded at $\nu_R = 10.0$ kHz. The satellite transition excitation and double–quantum reconversion were obtained using hard pulses of 1.5 and 1.0 μs, respectively, with a RF of 146 kHz. Two central transition's selective soft pulses of 30.5 (180^o) and 15.25 (90^o) μs corresponding to a RF of 8.2 kHz were employed for the double–quantum excitation and to convert the satellite transition to observable central transition, respectively; the recycle delay was set to 1.0 s. The software package DMFIT[40] was used for the curve fitting of the ^{11}B MAS NMR spectra based on the number of ^{11}B resonances observed in the STMAS spectrum.

Emission and excitation spectra were measured using a fluorescence spectrophotometer (Fluorlog, HORIBA JOBINYVON). The Commission Internationale de l'Eclairage (CIE) coordinates were calculated using a CIE analyzer (Ocean Optics, USB–2000). Decay measurements were performed with a tunable nanosecond optical–parametric–oscillator/Q–switch–pumped YAG:Nd^{3+} laser system (NT341/1/UV, Ekspla).

III. RESULTS AND DISCUSSION

A. XRD and SEM studies

The observed XRD patterns of $KCa_4(BO_3)_3$: xLn^{3+} are similar in the whole Ln^{3+} doping range. As an example, Fig. 1(a) shows the XRD patterns of $KCa_4(BO_3)_3$, $KCa_4(BO_3)_3$: 10%Dy^{3+} and $KCa_4(BO_3)_3$:5%Eu^{3+},5%Tb^{3+}. In the undoped parent sample, a mono–mineral composition was obtained with crystalline $KCa_4(BO_3)_3$ (JCPDS:01–75–3604) phase as evidenced by the minimal mismatch between the experimental and the simulated XRD data and absence of any significant misfits in the difference plot obtained using $Diffrac^{plus}$ TOPAS (Bruker AXS) software and the fitting has been performed using least–square methods. The resultant fitting of XRD patterns are shown in Fig. 1(b) and the resultant structural parameters have been refined simultaneously. The figure–of–merit (R), defines the mean standard deviation, suggests the good agreement between observed and calculated data and the obtained R factor values ($R_{exp} = 8.30$ $R_{wp} = 4.58$, $R_p = 3.52$ and GOF = 0.55) are well within the limits of experimental accuracy. The XRD data of $KCa_4(BO_3)_3$:Dy^{3+} and $KCa_4(BO_3)_3$:5%Eu^{3+}, 5%Tb^{3+} phosphors is in good agreement with that obtained for $KCa_4(BO_3)_3$ regardless of the dopant concentration as also certified by the Rietveld refinement. This implies towards the absence of any impurity phase in the as–prepared powders

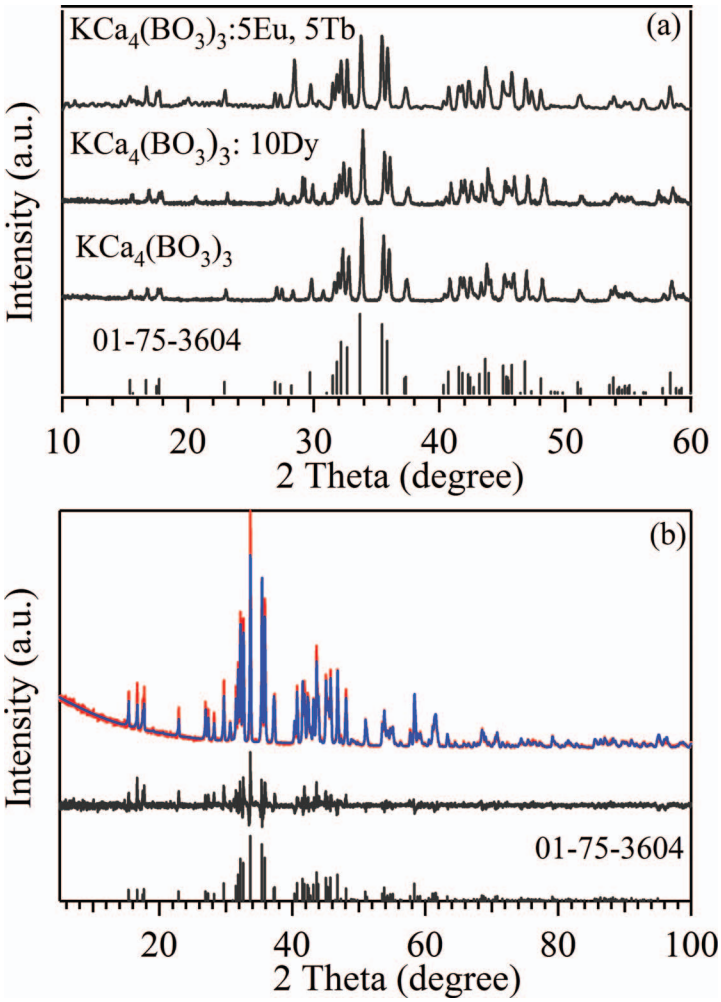

FIG. 1. (a) XRD patterns of undoped $KCa_4(BO_3)_3$ and 10 wt.% Dy^{3+} doped $KCa_4(BO_3)_3$ phosphor materials. The standard data for $KCa_4(BO_3)_3$ (JCPDS card no: 01–75–3604) are shown as a reference; (b) Observed (red), calculated (blue), and difference curves from the Rietveld refinement of $KCa_4(BO_3)_3$ phosphor.

and insignificant variations in the host crystal structure. Moreover, since the ionic radii of Dy^{3+} (105 pm), Eu^{3+} (109 pm) and Tb^{3+} (106 pm) are closer to Ca^{2+} (114 pm) instead of K^{+} (152 pm); it has been assumed that the non–centrosymmetric Ca^{2+} sites have been replaced by above mentioned ions in the $KCa_4(BO_3)_3$ crystal lattice.

On the basis of the detailed structural investigation of the two new types of borates, cubic and orthorhombic, isolated by Wu *et al*.,[36] it was evidenced that when the larger alkali metal cation was infixed to replace a smaller alkali metal ion, or reversely when a smaller alkaline earth metal cation was infixed to replace the larger alkali metal ions, the cubic structure became unstable and gave rise to the lower symmetric orthorhombic system. From the structural point of view, we need a flexible and stable host which will support the replacement of the internal cations with the desired metal ions without any considerable changes in the host lattice. For the non–centrosymmetric orthorhombic system, the larger cations can be easily replaced by the lanthanide ions, without changing the host crystal lattice. As the ionic radii of lanthanide ions (Dy^{3+} (105 pm), Eu^{3+} (109 pm), Tb^{3+} (106 pm)) are quite comparable to that of Ca^{2+} (114 pm), as well as their coordination geometries, the replacement of alkaline earth metal is easier and the host system becomes a perfect energy transfer system. The dopants occupy the interstitial positions symmetrically and interact with each other minimizing the resultant phonon energy within the host lattices while decreasing the luminescence quenching. It is worth to mention that, Wu and co–workers thoroughly investigated the structural

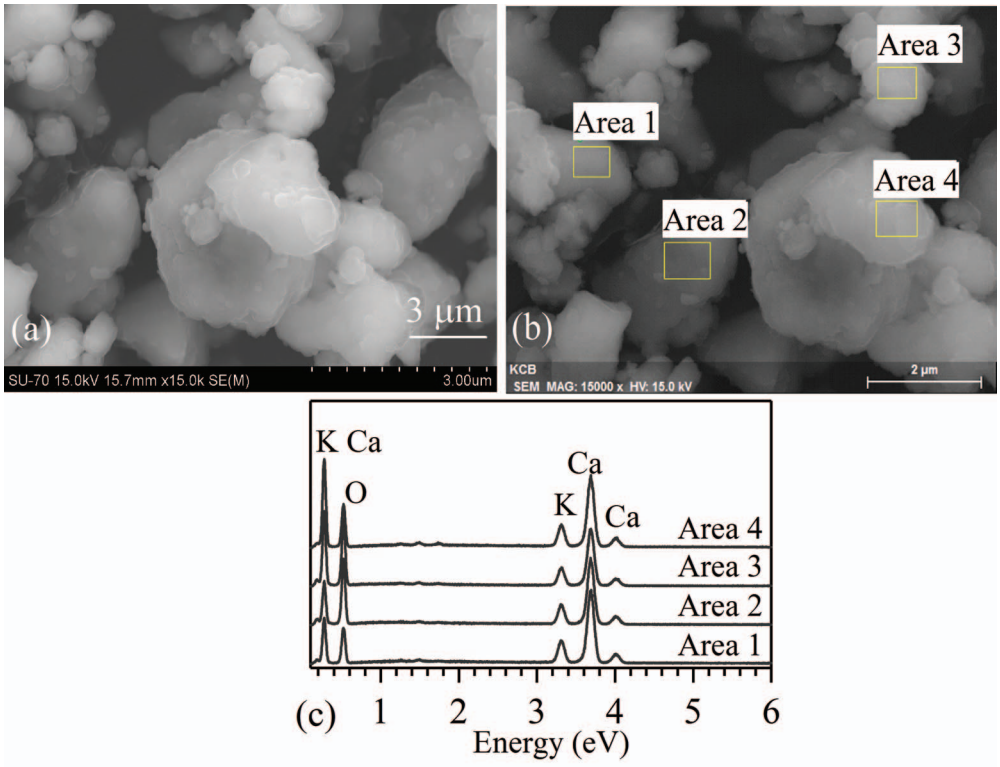

FIG. 2. (a) and (b) Surface morphology (SEM images) and (c) EDX analysis at four specified areas (as shown in Fig. 2(b)) for K and Ca of the $KCa_4(BO_3)_3$ phosphor synthesized at 800 ^oC for 7 hours.

correlation with energy transfer between Tm^{3+} and Dy^{3+} in $KSr_4(BO_3)_3$ host. Their structures were suggested to exhibit three Sr^{2+} centers and the dopants (Tm^{3+} and/or Dy^{3+}) preferably occupy the closest Sr^{2+} sites which are separated by a minimum distance of 3.38–3.35 Å. They also suggested that for an efficient energy transfer, a closest pair up is needed, being consistent with their results. From the structural refinement of our system we find that the closest distance among the Ca(1) and Ca(2) in $KCa_4(BO_3)_3$ is around 3.45 Å. This finding is consistent with the pairing up of (Eu^{3+} and/or Tb^{3+}) dopants, favoring an efficient energy transfer process.

The microstructural evolution of the as synthesized $KCa_4(BO_3)_3$ phosphor material as observed in SEM–EDX is presented in Fig. 2(a). The crystalline morphology of the as synthesized phosphor powders displayed micro granularity with their particle size varying between 1–10 μm. The particles appeared to be agglomerated indicating that the structures formed by solid state reaction have not been completely destroyed during the dry milling step. The excess amount of H_3BO_3 acting as flux during synthesis enhances the mobility of solid reactants and the formation of strong bonds within particle agglomerates. The consistent formation of $KCa_4(BO_3)_3$ was validated by EDX element analysis and results are given in Figure 2(b) and 2(c). These EDX results support well the XRD data. However, quantifying the individual species in the present host material by EDX element analysis is very difficult because of the inability of EDX detector for accurately detecting light elements as boron. But the constant proportionality between the K and Ca elements in the present EDX graphs broadly indicates the appropriate formation of the $KCa_4(BO_3)_3$ compound.

B. 3Q–MAS–NMR structural studies

^{11}B is a spin–3/2 nucleus with a relatively strong quadrupolar interaction. ^{11}B one–dimensional (1D) MAS NMR spectra are thus very often broadened by the anisotropic contribution (second–order quadrupolar broadening), which is not averaged out by MAS alone. To obtain highly resolved

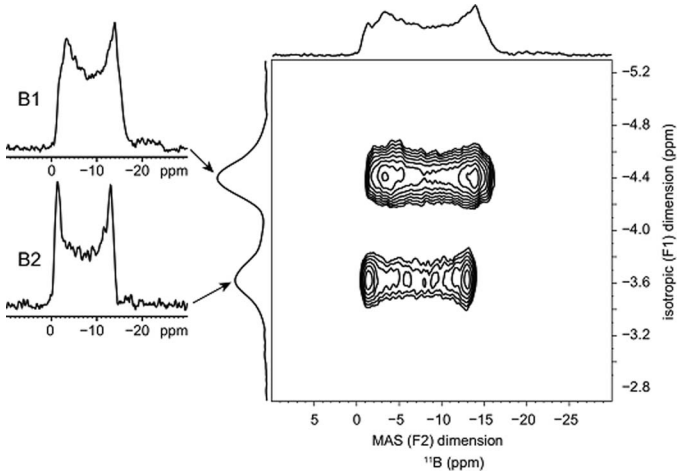

FIG. 3. 2D t1–split STMAS NMR spectra of $KCa_4(BO_3)_3$ along with the F1 and F2 projections. The second–order powder patterns of the two distinguishable boron sites are displayed on the left.

spectra for half–integer quadrupolar nuclei, 2D experiments such as STMAS (or MQMAS) must be employed to remove the anisotropies and yield isotropic line shapes. Therefore, this resolution enhancement allows the separation of overlapping resonances difficult to discriminate by simple MAS. In short, STMAS correlates a F2 dimension showing a low–resolution line shape, typical of second–order quadrupolar patterns similar to the ^{11}B MAS NMR spectrum and a F1 dimension giving a high–resolution isotropic dimension.

The crystal structure shows three different ^{11}B sites in $KCa_4(BO_3)_3$ in a 1:1:1 ratio. To achieve the separation of these sites we therefore acquired a STMAS spectrum on $KCa_4(BO_3)_3$. The 2D STMAS spectra of $KCa_4(BO_3)_3$ (Fig. 3) show at least two well–resolved ^{11}B peaks (B1 and B2) on its isotropic (F1) dimension. Both sites have very similar line shapes, stating that they present similar quadrupolar parameters (see below). This reflects an almost identical chemical environment for the boron species. The isotropic chemical shift (δ_{iso}), quadrupolar coupling constant (C_Q) and asymmetry parameter (η_Q) were obtained for site B1 ($\delta_{iso} = 1.40$ ppm, $C_Q = 2.62$ MHz and $\eta_Q = 0.15$) and site B2 ($\delta_{iso} = 2.75$ ppm, $C_Q = 2.63$ MHz and $\eta_Q = 0.06$) through simulation of their anisotropic projections shown in the left side of Fig. 3. The relative amounts of the two boron environments was determined using the 1D ^{11}B single–pulse MAS employing a small flip–angle (Fig. 4(a)) and the parameters (δ_{iso}, C_Q, η_Q) extracted from the STMAS spectra as usual practice. Ratios of 64.5% and 35.5% were obtained for site B1 and B2, respectively. This result corresponds approximately to a 2:1 (B1:B2) ratio between both sites and it is most likely that two ^{11}B resonances corresponding to two (almost) equivalent environments are overlapped (B1 and B3) while a third boron site (B2) being more symmetric ($\eta_Q = 0.06$; corresponding to a quadrupolar tensor very close to axial symmetry, *i.e.*, $\eta_Q \sim 0$) may be well separated from the other two. The presence of three crystallographic distinct boron sites in $KCa_4(BO_3)_3$ is therefore in agreement with the structure determined by Wu *et al.*[36] and with the PXRD results. The ^{11}B MAS NMR spectra of the doped samples (Fig. 4(b)(a) and 4(b)(b)) are significantly broadened, most likely due to the paramagnetic doping material Dy^{3+}. When comparing the spectra of these two samples with an artificially broadened spectrum (using exponential apodization) of the non–doped material (Fig. 4(b)(c)) we observe that, although broader, the spectra of the doped samples (Fig. 4(b)(a) and 4(b)(b)) are similar to the non–doped one (Fig. 4(b)(c)): the isotropic shifts are similar and for the 10% Dy doped sample, the positions of the distinguishable "horns" (due to the second–order quadrupolar interaction), at approximately −5 and −11 ppm (Fig. 4(b)(b)), are approximately the same as the ones shown by the ^{11}B MAS NMR spectrum of the broadened non–doped sample (Fig. 4(b)(c)). Therefore, the doped samples have comparable ^{11}B quadrupolar parameters and isotropic chemical shifts with respect to the non–doped sample, suggesting that their chemical surroundings are similar.

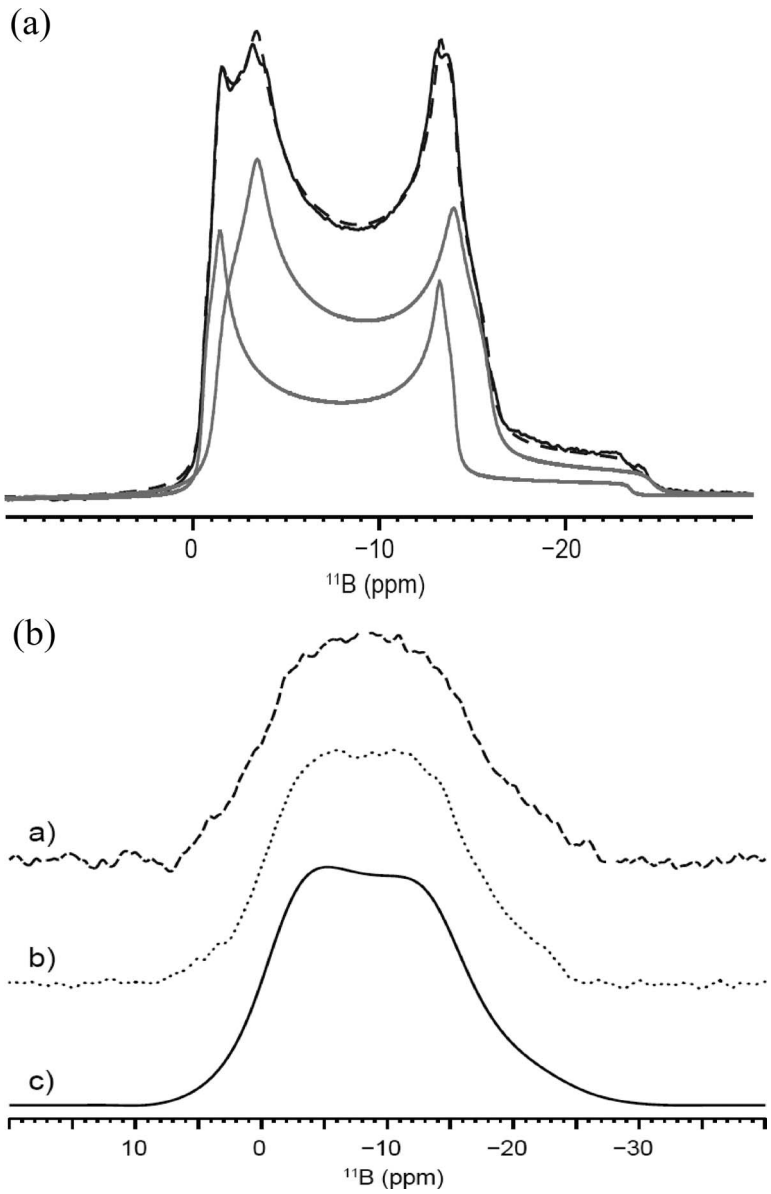

FIG. 4. (a) 1D MAS experimental spectra of $KCa_4(BO_3)_3$ (full black line) with the total line shape fit (black dotted line) and the two individual fitted sites (grey lines); (b) 1D MAS spectra of 5% Dy–doped (a), 10% Dy–doped (b) and un-doped $KCa_4(BO_3)_3$ (c) with additional artificial line–broadening (spectrum (c) is the same as Fig. 4(a) but with additional artificial line–broadening).

C. Photoluminescence studies

1. Photoluminescence of $KCa_4(BO_3)_3$:xDy^{3+} phosphors

Examples of photoluminescence excitation (PLE) and photoluminescence (PL) spectra are shown in Fig. 5(a) and 5(b) for the 5 wt.% Dy_2O_3 doped $KCa_4(BO_3)_3$ phosphor. The PLE spectrum presented in Fig. 5(a) was monitored at the dominant emission at 576 nm (Dy^{3+}:$^4F_{9/2} \rightarrow {}^6H_{13/2}$) and the spectra consists of two distinct regions. The first spectral region (200–280 nm) is associated with a broad band in the VUV region generated from charge transfer state of Dy–O bonding. The second region (280–500 nm) involves sharp bands corresponding to the characteristic transitions of individual Dy^{3+} ions. The excitation band at 350 nm, corresponds to $^6H_{15/2} \rightarrow {}^4M_{15/2}$, $^6P_{7/2}$ transitions, was found to be maximum, which is mainly utilized to monitor the Dy^{3+} emission

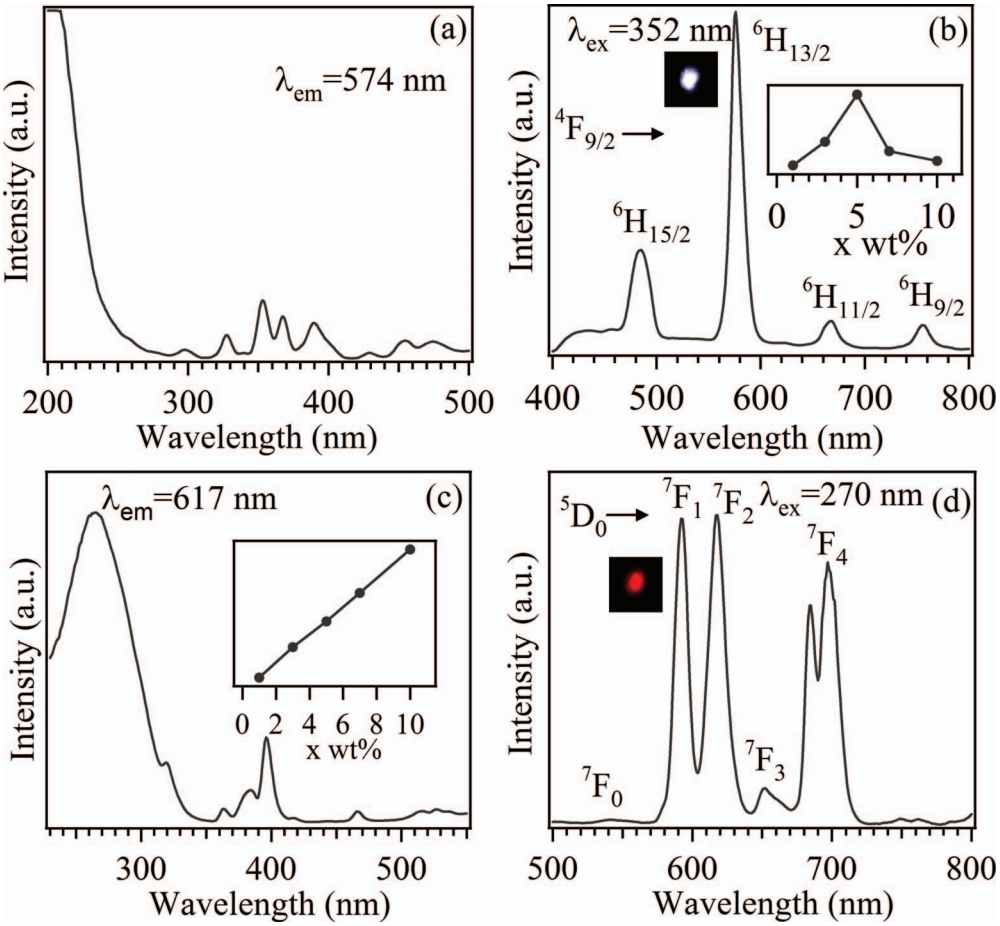

FIG. 5. (a) PLE (λ_{em} = 575 nm) and (b) PL (λ_{ex} = 350 nm) spectra of 5 wt% Dy^{3+} doped $KCa_4(BO_3)_3$ phosphor. Inset of Fig (b) shows the variation of 575 nm emission intensity variation with respect to Dy^{3+} concentration and PL digital image for 5 % Dy^{3+} doped $KCa_4(BO_3)_3$ phosphor. (c) PLE (λ_{em} = 615 nm) and (d) PL (λ_{ex} = 270 nm) spectra of 10 wt% Eu^{3+} doped $KCa_4(BO_3)_3$ phosphor. Inset of Fig (c) shows the variation of 615 nm emission intensity variation with respect to Eu^{3+} concentration and PL image for 10 % Eu^{3+} doped $KCa_4(BO_3)_3$ phosphor.

spectrum. The emission spectra (Fig. 5(b)) contains dominant emissions at 482 nm (blue) and 576 nm (yellow) and other low intense peaks at 670 nm (red) and 750 nm, which are attributed to the transitions from $^4F_{9/2}$ to various energy levels $^6H_{15/2}$, $^6H_{13/2}$, $^6H_{11/2}$ and $^6H_{9/2}$, respectively. In general, the yellow emission is due to magnetic dipole originated hypersensitive transition and is dominant when Dy^{3+} ions are situated at low–symmetry sites with no inversion centres.[11] In the present study, the yellow emission at 576 nm was found to be predominant over blue (482 nm) emission (see Fig. 5(b)), suggests that the Dy^{3+} ions are situated away from inversion symmetry, and this observation is consistent with the structural study that Dy^{3+} occupies the non–centrosymmetric position of Ca^{2+}. In the present case, since the ionic radius of Dy^{3+} (105 pm) is closer to Ca^{2+} (114 pm) ionic radius in comparison to that of K^+ (152 pm), therefore Dy^{3+} might have preference for substituting the Ca^{2+} ions in the lattice. The occupation of Dy^{3+} ion into Ca^{2+} sites in $KCa_4(BO_3)_3$ host eventually generates number of oxygen vacant sites, thereby lead to expand the lattice and lower the crystal density. According to Lopez *et al.*,[41] oxygen vacancies might be useful to enhance the rare-earth ion emission by acting as sensitizers for efficient energy transfer from charge transfer states to the rare earth ions. However, the crystallinity of the host would be inevitably destroyed by these excess oxygen vacancies, which may eventually lead to quenching of rare earth ion emission.

In order to investigate the emission intensity variation with respect to the content of Dy^{3+} ion doping, specially to observe the effect of local surroundings on Dy^{3+}, several $KCa_4(BO_3)_3$ phosphors

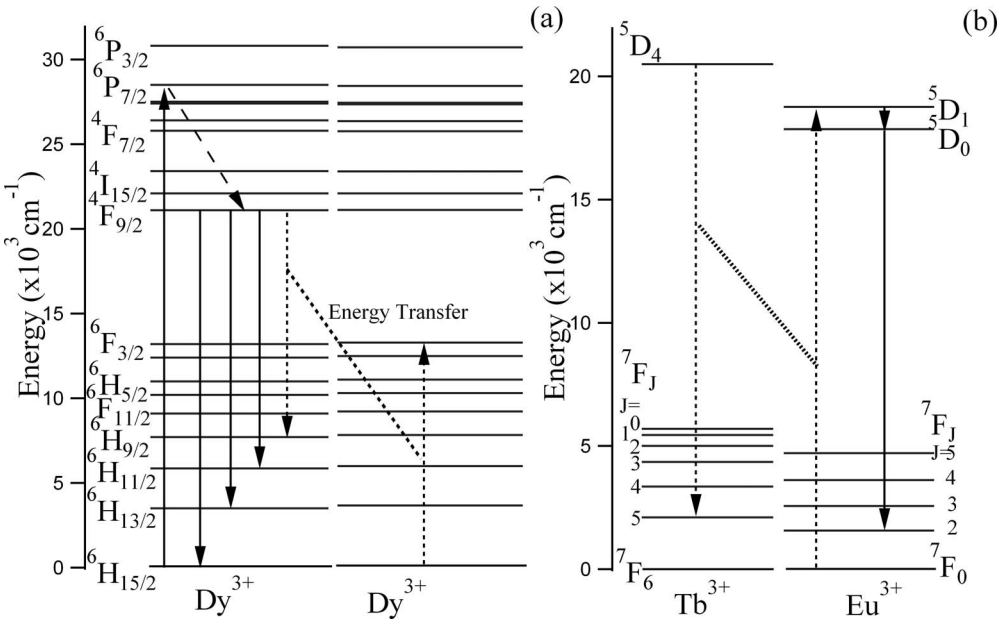

FIG. 6. (a) Energy level diagrams, visible emission transition for Dy^{3+}, and the resonance energy transfer among Dy^{3+} ions. (b) Energy level diagrams and energy transfer behaviour of Tb^{3+} and Eu^{3+} ions in $KCa_4(BO_3)_3$.

with various dopant concentrations of Dy^{3+} (1% to 10%) were prepared and their yellow emission intensities were monitored under 350 nm excitation (inset of Fig. 5(b)). As seen, the optimal value for the maximum photoluminescence intensity was found to be 5% of Dy^{3+} ion concentration. The emission quenching at higher concentration is due to the inter–ion energy transfer and for this reason, the critical separation between donor and acceptors has to be estimated. The critical energy transfer distance R_c between the activators could be estimated from the equation:[42]

$$R_c = 2(3V/4\pi X_c Z) \tag{1}$$

where X_c is the critical concentration in mol.%, Z is the number of cations in the unit cell and V is the volume of the unit cell. By considering the experimental and analytic values of X_c, Z and V [5 wt.% (0.022 mol.%), 16 and 744.637 Å respectively, the critical transfer distance of Dy^{3+} in the present phosphor is estimated to be about 15.93 Å.

The schematic energy levels of Dy^{3+} ions are presented in Fig. 6(a) according to the calculated values of Carnall *et al.*[43] When the 4f higher energy levels of Dy^{3+} ions are excited at 350 nm, the initial population nonradiatively relaxes to the lower energy levels by phonon–assisted processes until it arrives to the $^4F_{9/2}$ level, then radiatively deactivates giving rise to strong blue and yellow emissions and other weak red-end emissions. With the elevated Dy^{3+} content, these characteristic emissions increase upto $x = 5\%$, and subsequently decreases drastically.

The photoluminescence decay curves of different $KCa_4(BO_3)_3$: x Dy^{3+} phosphors for the 575 nm emission with 350 nm excitation were also recorded and the resultant decay curves could be fitted by a single exponential function:

$$I(t) = I_0 e^{-t/\tau} \tag{2}$$

where I_0 is the initial intensity at $t = 0$, and τ is the decay lifetime. The corresponding decay times in $KCa_4(BO_3)_3$:$x$$Dy^{3+}$ phosphor was 0.51, 0.52, 0.54, 0.49 and 0.48 ms for 1%, 3%, 5%, 7% and 10% Dy^{3+}, respectively. The lifetime values increased with the increase of Dy^{3+} content up to 5%, and then decreases as a result of concentration quenching. The decay curves of $KCa_4(BO_3)_3$:$x$$Dy^{3+}$ phosphors were very similar to each other even for higher doping concentrations of Dy^{3+}. The best fit results of single component exponential decay indicate uniform doping in the present host.

TABLE I. CIE Color coordinates of $KCa_4(BO_3)_3:Ln^{3+}$ (Ln:Tb, Eu and Dy) phosphors ($\lambda_{ex} = 350$ nm).

Wt% of Ln^{3+}	Y/B	CIE	
		X	Y
1% Dy^{3+}	1.61	0.353	0.369
3% Dy^{3+}	1.64	0.359	0.390
5% Dy^{3+}	3.33	0.381	0.398
7% Dy^{3+}	1.51	0.332	0.381
10% Dy^{3+}	1.51	0.353	0.392
5%Eu^{3+}	–	0.594	0.400
5%Tb^{3+}	–	0.365	0.524
5%Eu^{3+} –5%Tb^{3+}	–	0.360	0.400

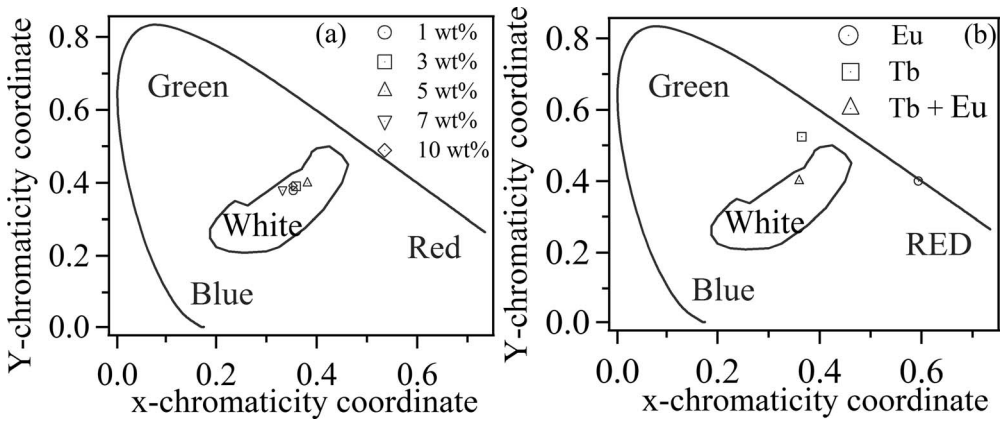

FIG. 7. (a) CIE coordinate diagram of $KCa_4(BO_3)_3:x\%Dy^{3+}$ phosphors ($\lambda_{ex} = 350$ nm). (b) CIE coordinate diagram of $KCa_4(BO_3)_3$:5%Eu^{3+}, $KCa_4(BO_3)_3$:5%Tb^{3+} and $KCa_4(BO_3)_3$:5%Eu^{3+}–5%Tb^{3+} phosphors ($\lambda_{ex} = 350$ nm).

The Y/B intensity ratio (listed in Table I) of Dy^{3+} was found to assume different values, from 1.5 to 3.33 when the concentration of Dy^{3+} is changed, indicating that the crystal field environment surrounding the Dy^{3+} ions is changing abruptly with the incorporated amount of Dy^{3+}. Hence, white light emission can be achieved from $KCa_4(BO_3)_3:xDy^{3+}$ phosphors as confirmed by CIE coordinates. The CIE chromaticity coordinates of $KCa_4(BO_3)_3:xDy^{3+}$ phosphors with different Dy^{3+} concentrations were calculated from the emission spectra (Fig. 5(b)) and presented in Fig. 7(a) and the corresponding co–ordinates are listed in Table I. The values of color coordinates are nearer to pure white–light whose color coordinates are $x = y = 0.3333$. This fact suggests that white–light could be achieved by appropriately controlling the Dy^{3+} concentration thereby adjusting the ratio of dominant blue and yellow emissions. To compare the different white emissions, the whiteness parameter (W) was calculated according to the equation.[44]

$$W = Y + 800(x_R - x) + 1700(y_R - y) \quad (3)$$

where, Y is the tristimulus value, (x, y) are the chromaticity coordinates in the CIE 1931 color space and $(x_R, y_R) = (0.33, 0.33)$ are the chromaticity coordinates of the perfect white light emitter. A perfect white give W = 100%. Our results shows that the emission of $KCa_4(BO_3)_3$:1%Dy^{3+} phosphor is the nearest of perfect white (W = 84%), which is also evident to the naked eye (inset of Fig. 5(b)). In order to verify the potentiality as one of the effective white–light emitting phosphors for the white LEDs, the external quantum efficiency (EQE) of this phosphor was also estimated according to the process adopted by Hirosaki *et al.*[45] For $KCa_4(BO_3)_3$:1%Dy^{3+} phosphor, the EQE was determined to be 52% upon excitation at 350 nm and. However, the experimental conditions and the composition of the phosphor must be optimized for further improvement in the efficiency values. It is worth to mention that the quantum efficiencies in general are influenced by the lattice defects, stoichiometric

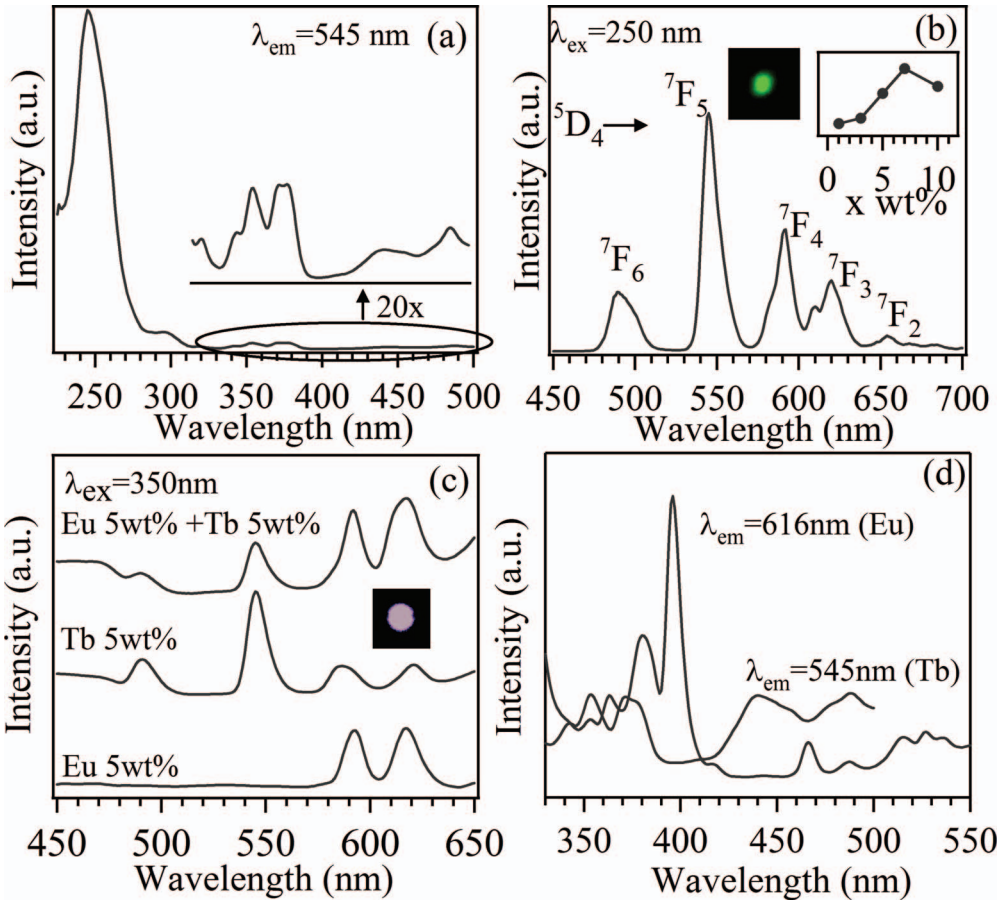

FIG. 8. (a) PLE spectra (λ_{em} = 545 nm) and (b) PL spectra (λ_{ex} = 250 nm) of 7 wt.% Tb^{3+} doped $KCa_4(BO_3)_3$ phosphor. Inset in Fig. 8(b) shows the variation of 545 nm emission intensity with respect Tb^{3+} concentration and PL digital image for 7 % Tb^{3+} doped $KCa_4(BO_3)_3$ phosphor. (c) PL (λ_{ex} = 350 nm) and (d) PLE spectra of $KCa_4(BO_3)_3$:5%Eu^{3+}–5%Tb^{3+} and $KCa_4(BO_3)_3$:5%Eu^{3+},5%Tb^{3+} phosphors. Inset in (c) shows PL digital image for 5 % Tb^{3+}–5 % Eu^{3+} codoped $KCa_4(BO_3)_3$ phosphor.

excess, nonradiative deactivation centers and self–absorption.[46] Post–synthesis annealing is usually used to improve the crystallinity, surface morphology and stoichiometry to improve the phosphor's emission efficiency. Furthermore, the phosphor absorption at the long–wavelength range needs to be reduced to avoid self–absorption.[46]

2. Photoluminescence of Eu^{3+}, Tb^{3+} singly and codoped $KCa_4(BO_3)_3$ phosphors

Figures 5(c) and 5(d) depicted the PLE and PL spectra of $KCa_4(BO_3)_3$:$x$$Eu^{3+}$ phosphor, respectively. In the PLE spectrum of Eu^{3+} (see Fig. 5(c)), monitored at the emission of 615 nm, the strong UV broad band (~270 nm) can be assigned to the charge transfer transition between Eu^{3+} and O^{2-}, and other sharp peaks are originating from the *f–f* transitions of Eu^{3+} ions. The excitation peaks ranging from 350 to 500 nm can be identified as the intrinsic of Eu^{3+} transitions from $^7F_0$ to $^5L_6$ and $^5D_2$. Upon excitation at 270 nm, the PL spectra (Fig. 5(d)) shows intense transition lines from the excited $^5D_0$ level of Eu^{3+} ions and their transition assignments are appropriately assigned. Two main characteristic peaks from $^5D_0 \rightarrow {}^7F_1$ (orange, 591 nm) and $^5D_0 \rightarrow {}^7F_2$ (red, 615 nm) are dominant. The red emission at 615 nm increases systematically with the Eu^{3+} content (Fig. 5(c)) suggesting the minimum concentration quenching effects.

Figs. 8(a) and 8(b) display the PLE and PL spectra of $KCa_4(BO_3)_3$:$x$$Tb^{3+}$ (x = 1% to 10 wt.%), respectively. The PLE spectrum (Fig. 8(a)) consists of an intense broad band peaked at 250 nm

and generated from the spin–allowed $^4f_8 \rightarrow {}^4f_7$ 5d transition ($\Delta S = 0$) of Tb^{3+}. The sharp but low intense excitation peaks in the 300–500 nm wavelength region are within the Tb^{3+};$^4f_8$ electron configuration. The characteristic emission lines of Tb^{3+}ions, $^5D_4 \rightarrow {}^7F_J$ (J = 3, 4, 5, 6) transitions are clearly visible with the prominent green emission $^5D_4 \rightarrow {}^7F_5$ (545 nm), when these phosphors are exited at 250 nm (Fig. 8(b)). Upon investigating the dependence of corresponding PL intensity as a function of Tb^{3+} concentration (inset of Fig. 8(b)), we derived the optimal dopant concentration of Tb^{3+} as 7%.

Interestingly, the co–doped phosphor system $KCa_4(BO_3)_3$:Eu^{3+} – Tb^{3+} showed prominent and equally intense orange–red (Eu^{3+}) and green emissions (Tb^{3+}). Fig. 8(c) shows such emission from Eu^{3+}–Tb^{3+} phosphor (λ_{ex} = 350 nm), where the individual PL spectra for Eu^{3+} and Tb^{3+} doped phosphors are also shown for comparison. As seen in the spectrum (Fig. 8(c)), the dominant orange–red and green emissions are due to respective Eu^{3+} and Tb^{3+} ions, giving rise to near white–light emission. With the addition of Eu^{3+}, the orange–red emissions of Eu^{3+} systematically increases, at the expense of green emission (Tb^{3+}:$^5D_4 \rightarrow {}^7F_5$) intensity. As it is known, the tricolor combination (red, green and blue or any mixture of two of them) in different ratios can show white light emission, therefore, different mixing ratios of Eu^{3+}, Tb^{3+} ions are attempted in the present study. When the proportions of Eu^{3+} and Tb^{3+} codoping ions are 5/5 wt.% (shown in Fig. 8(c)) the near white–light emission was achieved due to the equal contribution of intensities of red, orange and green emissions, which was supported by the efficient energy transfer from Tb^{3+} to Eu^{3+}. Excitation spectra for $KCa_4(BO_3)_3$:Eu^{3+}–Tb^{3+} phosphor obtained by monitoring the $^5D_0 \rightarrow {}^7F_2$ transition of Eu^{3+} (615 nm) and the $^5D_4 \rightarrow {}^7F_5$ transition of Tb^{3+} (545 nm) are shown in Fig. 8(d). The overlapping excitation peaks in the region between 350–375 nm clearly indicates the close proximity of energy levels of individual ions for efficient charge transfer between Tb^{3+} and Eu^{3+} during near UV excitations. Fig. 6(b) shows the schematic energy level diagram to understand such energy transfer mechanism between Tb^{3+} and Eu^{3+} ions. During the relaxation process of Tb^{3+} ions to their ^7F_J states, the energy being partially transferred to ground states of Eu^{3+} ions and eventually excites the electrons from the ground states to $^5D_1$ level, as shown by the dashed lines (Fig. 6(b)). The following equation explains the energy transfer process:

$$^5D_4(Tb^{3+}) + {}^7F_0(Eu^{3+}) \rightarrow {}^7F_5(Tb^{3+}) + {}^5D_1(Eu^{3+}) \quad (4)$$

To gain further insight into the energy transfer mechanisms, the luminescent decay of Tb^{3+}:541 nm and Eu^{3+}:616 nm emissions were also measured. The decay curves of the Tb^{3+} and Eu^{3+} singly doped phosphors can be well fit by the single exponential (equation 2). The decay life times extracted from the fitted curve of 5%Tb^{3+} and 5%Eu^{3+} singly doped phosphors are found to have 0.451 ms and 0.463 ms respectively. The lifetime of Tb^{3+};545 nm emission in Eu^{3+}–Tb^{3+} codoped sample (0.424 ms) is slightly shorter than the singly doped phosphor, while that of Eu^{3+};615 nm (0.478 ms) was little larger than the single Eu^{3+} doped phosphor. The corresponding PL decay profiles of the Tb^{3+}; 545 nm and Eu^{3+}; 615 nm emissions of the Eu^{3+}–Tb^{3+} codoped sample have been depicted in Fig. 9(a). In general, the PL decay of the singly doped samples resulted into a single exponential whereas the codoped phosphor was found to have a doubled exponential nature. Such double exponential decay curves can be fitted using the following equation:[47]

$$I(t) = I_1 e^{-t/\tau_1} + I_2 e^{-t/\tau_2} \; with \; I_1 + I_2 = 1 \quad (5)$$

where $I(t)$ is the intensity of luminescence for a time, τ_1 and τ_2 are the short and long lifetimes corresponding to the intensity coefficients I_1 and I_2, respectively. The average lifetime, hence defined as $\tau_{av} = (I_1\tau_1^2 + I_2\tau_2^2) / (I_1\tau_1 + I_2\tau_2)$.[48] Clear deviation of PL decay from single exponential behavior suggests the predominance of ion–ion interactions and energy transfer phenomena between Eu^{3+} and Tb^{3+} ions. This resulting into have relatively fast and slow PL decay components.

The observed color compensated white emission in the $KCa_4(BO_3)_3$: Eu^{3+},Tb^{3+} phosphor can be further confirmed by the CIE coordinates. As seen in the CIE diagram (Fig. 7(b)), the emission color of $KCa_4(BO_3)_3$: 5% Eu^{3+}–5% Tb^{3+} was observed to be in the near white–light region (0.36, 0.40) very close to that of pure white–light (0.33, 0.33). The PL digital image (inset of Fig. 8(c)) recorded by 350 nm excitation also confirms the near white–light. The external quantum efficiency of the PL estimates to be about 43%. The above results clearly see demonstrates near white–light due

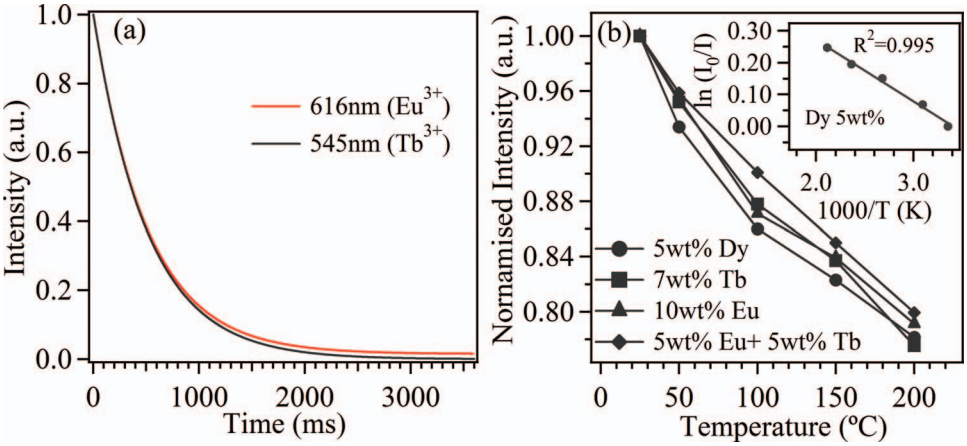

FIG. 9. (a) PL emission decay curves of $KCa_4(BO_3)_3$:5%Eu^{3+}–5%Tb^{3+} phosphor recorded for the individual green (545 nm, $^5D_4 \rightarrow {}^7F_5$ of Tb^{3+}) and red (615 nm, $^5D_0 \rightarrow {}^7F_2$ of Eu^{3+}) emissions. (b) Thermal quenching data of 5% Dy^{3+}, 7% Tb^{3+}, 10% Eu^{3+}, and 5% Eu^{3+} – 5% Tb^{3+} doped $KCa_4(BO_3)_3$ excited at 360 nm. Inset shows the plot of ln(I_0/I) *vs* 1/T for the 5% Dy^{3+} doped phosphor (see text).

to the combined emissions of the Eu^{3+} and Tb^{3+} ions, supported by partial energy transfer between the ions. Hence, $KCa_4(BO_3)_3$:Eu^{3+},Tb^{3+} phosphor system would potentially be used as white light emitting phosphor and these findings would certainly encourage more studies on the luminescence properties for its further optimization and simplified white–light generation.

D. Thermal stability measurements

For device applications, high thermal stability of phosphor is one of the requirements to avoid any transformations in the chromaticity and brightness. Fig. 9(b) shows the temperature dependence of the luminescence intensity for selective phosphors (5%Dy^{3+}, 5%Eu^{3+}, 5%Tb^{3+} and 5%Eu^{3+}–5%Tb^{3+} codoped phosphors) excited at 350 nm. At 200 °C, all the phosphors retain more than 75% of the intensity, which is favorable feature for LED applications. The activation energy (E_a) can be extracted from the expression:[5]

$$\ln(I/I_0) = \ln A - E_a/kT. \quad (6)$$

Where, I_0 and I are the luminescence intensity at room and testing temperatures, respectively; A is a constant; and k is the Boltzmann constant (8.617×10^{-5} eV K^{-1}). From eq. (6), we determined E_a to be 0.017, 0.016, 0.017 and 0.015 eV for 5%Dy^{3+}, 5%Eu^{3+}, 5%Tb^{3+} singly doped and 5%Eu^{3+}, 5%Tb^{3+} codoped $KCa_4(BO_3)_3$ phosphors, respectively. As an example, the long (I_0/I) *vs* 1000/T fitting for the calculation of activation energy of $KCa_4(BO_3)_3$:5%Dy^{3+} is also shown as inset of Fig. 9(b).

IV. CONCLUSIONS

Dy^{3+}, Eu^{3+}, Tb^{3+} singly doped and Eu^{3+}–Tb^{3+} codoped $KCa_4(BO_3)_3$ phosphors were successfully fabricated from solid–state reactions for the purpose of white-light LEDs. Dy^{3+} doped $KCa_4(BO_3)_3$ emits bright blue and yellow emissions upon excitation near UV range. As confirmed from chromatic analysis, the intensity ratios of prominent yellow and blue color emissions can be conveniently controlled by simply varying the Dy^{3+} concentrations to achieve the desired near white-light emission. More importantly, a systematic study on the PL properties of $KCa_4(BO_3)_3$:Ln^{3+} (Ln = Eu, Tb) has been explored under near UV excitation in order to obtain multicolour-emitting phosphors. The 5 wt.% Eu^{3+} and 5 wt.% Tb^{3+} co–doped phosphor showed near white light emission upon near UV excitation. This was possible due to the partial energy transfer from Tb^{3+} to Eu^{3+}, as

confirmed by the PL decay analysis. In the meantime, present phosphor systems exhibited adequate thermal stability even at 200 °C. This broadly suggests that the current phosphors can be very suitable for LED applications. Overall, the strong absorption in UV and near UV range, efficient multicolour emission including white light, moderate decay time makes it a potential candidate for efficient white light LEDs.

ACKNOWLEDGMENTS

This study was financially supported by the University of Aveiro, CICECO, and FCT, Portugal (PTDC/CTM–CER/114209/2009). The support from CICECIO, University of Aveiro, is acknowledged. This work partly supported by Department of Information Technology (DIT), Govt. of India, under Photonics Development Program (ref: 12(1)/2008–PDD), NanoResearch Facility and High–Impact Research Schemes of IIT Delhi.

[1] S. Pimputkar, J. S. Speck, S. P. DenBaars, and S. Nakamura, Nat. Photonics **3**, 180 (2009).
[2] E. F. Schubert and J. K. Kim, Science **308**, 1274 (2005).
[3] T. Hashimoto, F. Wu, J. S. Speck, and S. Nakamura, Nat. Mater. **6**, 568 (2007).
[4] G. Li, D. Geng, M. Shang, C. Peng, Z. Chenga, and J. Lin, J. Mater. Chem. **21**, 13334 (2011).
[5] W. R. Liu, C. H. Huang, C. P. Wu, Y. C. Chiu, Y. T. Yeh, and T. M. Chen, J. Mater. Chem. **21**, 6869 (2011).
[6] X. Liu, Y. Liu, D. Yan, H. Zhu, C. Liu, C. Xu, Y. Liu, and X. Wang, J. Mater. Chem. **22**, 16839 (2012).
[7] T. S. Chan, R. S. Liu, and I. Baginskiy, Chem. Mater. **20**, 1215 (2008).
[8] A. A. Reddy, S. Das, S. Ahmad, S. Babu, J. M. F. Ferreira, and G. Vijaya Prakash, RSC Advances **2**, 8768 (2012).
[9] Y. Q. Li, A C. A. Delsing, G. D. With, and H. T. Hintzen, Chem. Mater. **17**, 3242 (2005).
[10] M. S. Wang, S. P. Guo, Y. Li, L. Z. Cai, J. P. Zou, G. Xu, W. W. Zhou, F. K. Zheng, and G. C. Guo, J. Am. Chem. Soc. **131**, 13572 (2009).
[11] S. Das, A. A. Reddy, S. S. Babu, and G. Vijaya Prakash, J. Mater. Sci. **46**, 7770 (2011).
[12] J. Zhang, Z. Zhang, Z. Tang, Y. Tao, and X. Long, Chem. Mater. **14**, 3005 (2002).
[13] K. B. Kim, Y. I. Kim, H. G. Chun, T. Y. Cho, J. S. Jung, and J. G. Kang, Chem. Mater. **14**, 5045 (2002).
[14] S. Oshio, T. Matsuoka, S. Tanaka, and H. Kobayashi, J. Electrochem. Soc. **145**, 3903 (1998).
[15] Y. Shimomura, T. Kurushima, and N. Kijima, J. Electrochem. Soc. **154**, J234 (2007).
[16] Y. Shimomura, T. Honma, M. Shigeiwa, T. Akai, K. Okamoto, and N. Kijima, J. Electrochem. Soc. **154**, J35 (2007).
[17] A. A. Setlur, W. J. Heward, Y. Gao, A. M. Srivastava, R. G. Chandran, and M. V. Shankar, Chem. Mater. **18**, 3314 (2006).
[18] A. A. Setlur, W. J. Heward, M. E. Hannah, and U. Happek, Chem. Mater. **20**, 6277 (2008).
[19] W. B. Im, N. George, J. Kurzman, S. Brinkley, A. Mikhailovsky, J. Hu, Bradley F. Chmelka, S. P. DenBaars, and R. Seshadri, Adv. Mater. **23**, 2300 (2011).
[20] M. S. Wang, S. P. Guo, Y. Li, L. Z. Cai, J. P. Zou, G. Xu, W. W. Zhou, F. K. Zheng, and G. C. Guo, J. Am. Chem. Soc. **131**, 13572 (2009).
[21] V. Bachmann, C. Ronda, O. Oeckler, and W. Schnick, Chem. Mater. **21**, 316 (2009).
[22] J. A. Kechele, C. Hecht, O. Oeckler, J. S. auf der Günne, P. J. Schmidt, and W. Schnick, Chem. Mater. **21**, 1288 (2009).
[23] Y. Q. Li, A. C. A. Delsing, G. de With, and H. T. Hintzen, Chem. Mater. **17**, 3242 (2005).
[24] R. J. Xie, N. Hirosaki, K. Sakuma, Y. Yamamoto, and M. Mitomo, Appl. Phys. Lett. **84**, 5404 (2004).
[25] T. Suehiro, N. Hirosaki, R. J. Xie, and M. Mitomo, Chem. Mater. **17**, 308 (2005).
[26] H. S. Yoo, W. B. Im, S. Vaidyanathan, B. J. Park, and D. Y. Jeon, J. Electrochem. Soc. **155**, J66 (2008).
[27] Y. S. Hu, W. D. Zhuang, H. Q. Ye, S. S. Zhang, Y. Fang, and X. W. Huang, J. Lumin. **111**, 139 (2005).
[28] Q. H. Zhang, J. Wang, R. J. Yu, M. Zhang, and Q. Su, Electrochem. Solid State Lett. **11**, H335H (2008).
[29] J. Liu, H. Z. Lian, C. S. Shi, and J. Y. Sun, J. Electrochem. Soc. **152**, G880 (2005).
[30] T. R. N. Kutty, Mater. Res. Bull. **25**, 343 (1990).
[31] L. Wang and Y. Wang, Mater. Sci. Eng., B **139**, 232 (2007).
[32] Y. Zhang and Y. Li, J. Alloys Compd. **384**, 88 (2004).
[33] H. Liang, H. Lin, G. Zhang, P. Dorenbos, and Q. Su, J. Lumin. **131**, 194 (2011).
[34] X. Zhang, X. Qiao, and H. J. Seo, Curr. Appl. Phys. **11**, 442 (2011).
[35] C. Guo, H. Jing, and T. Li, RSC Advances **2**, 2119 (2012).
[36] L. Wu, X. L. Chen, Y. P. Xu, and Y. P. Sun, Inorg. Chem. **45**, 3042 (2006).
[37] Y. R. Shi, Y. H. Wang, and Z. G. Yang, J. Alloys Compd. **509**, 3128 (2011).
[38] Q. Su, Z. W. Pei, L. S. Chi, H. J. Zhang, Z. Y. Zhang, and F. Zou, J. Alloys Compd. 192 (1993).
[39] J. Trebosc, J. P. Amoureux, and Z. Gan, Solid State Nucl. Magn. Reson. **31**, 1 (2007).
[40] D. Massiot, F. Fayon, M. Capron, I. King, S. Le Calvé, B. Alonso, J. O. Durand, B. Bujoli, Z. Gan, and G. Hoatson, Magn. Reson. Chem. **40**, 70 (2002).
[41] O. A. Lopez, J. Mckittrick, and L. E. Shea, J. Lumin. **71**, 1 (1997).
[42] G. Blasse, J. SolidState Chem. **62**, 207 (1986).

[43] W. T. Carnall, P. R. Fields, and K. Rajnak, J. Chem. Phys. **49**, 4424 (1968).
[44] CIE Colorimetry Technical Report, CIE Central Bureau, Vienna, 3rd edn, 2004, vol. 15.
[45] N. Hirosaki, R. J. Xie, and K. Kimoto, Appl. Phys. Lett. **86**, 211905 (2005).
[46] C. Chartier, C. Barthou, P. Benalloul, S. Chenot, and J. Frigerio, J. Cryst. Growth **256**, 305 (2003).
[47] L. Li, Z. Zhou, H. Tian, D. Gong, Z. Yang, and Y. Yang, J. Appl. Phys. **108**, 043520 (2010).
[48] N. Yaiphaba, R. S. Ningthoujam, N. Shanta Singh, R. K. Vatsa, N. Rajmuhon Singh, Sangita Dhara, N. L. Misra, and R. Tewari, J. Appl. Phys. **107**, 034301 (2010).